Phased Reconnaissance Approach to Documenting Landslides Following the 2016 Central Italy Earthquakes

Kevin W. Franke, M. EERI, Bret N. Lingwall, M. EERI, Paolo Zimmaro, M. EERI, Robert E. Kayen, M. EERI, Paolo Tommasi, Filiberto Chiabrando, and Antonio Santogo

The 2016 Central Italy earthquake sequence caused numerous landslides over a large area in the Central Apennines. As a result, the Geotechnical Extreme Events Reconnaissance Association (GEER) organized post-earthquake reconnaissance missions to collect perishable data. Given the challenging conditions following the earthquakes, the GEER team implemented a phased reconnaissance approach. This paper illustrates this approach and how it was used to document the largest and most impactful seismically induced landslides. This phased approach relied upon satellite-based interferometric damage proxy maps, preliminary published reports of observed landslides, digital imaging from small unmanned aerial vehicles (UAVs), traditional manual observations, and terrestrial laser scanning. Data collected from the reconnoitered sites were used to develop orthophotos and meshed three-dimensional digital surface models. These products can provide valuable information such as accurate measurements of landslide ground movements in complex topographic geometries or boulder runout distances from rock falls. The paper describes three significant landslide case histories developed and documented with the phased approach: Nera Valley, Village of Pescara del Tronto, and near the villages of Crognaleto and Cervaro. [DOI: 10.1193/082117EQS165M]

INTRODUCTION

Six large earthquakes occurred in the Apennine Mountains near Amatrice and Norcia in Central Italy on 24 August, 26 August, 26 October, and 30 October 2016. The moment magnitudes (**M**) of these events were 6.1, 5.3, 4.8, 5.4, 5.9, and 6.5, respectively. This paper will primarily focus on the three largest earthquake events: the **M**6.1 (24 August), the **M**5.9 (26 October), and the **M**6.5 (30 October) events. Because of the mountainous terrain of

a) Department of Civil and Environmental Engineering, Brigham Young University, Provo, UT 84602; Email: kfranke@et.byu.edu (KWF, corr. author)

b) Department of Civil and Environmental Engineering, South Dakota School of Mines and Technology, Rapid City, SD 57701

c) Department of Civil and Environmental Engineering, University of California, Los Angeles, Los Angeles, CA 90095

d) United States Geological Survey (USGS), Menlo Park, CA

e) Istituto di Geologia Ambientale e Geoingegneria (IGAG), CNR, Rome, Italy

f) Dipartimento di Architettura e Design, Politecnico di Torino, Torin, Italy

g) Dipartimento di Ingegneria Civile, Edile e Ambientale, Università degli Studi di Napoli Federico II, Naples, Italy

Central Italy, the large number of existing landslides affecting the region, and the large earthquake accelerations, numerous seismic-induced landslides occurred during each earthquake event. According to the Cruden and Varnes (1996) classification updated by Hungr et al. (2014), these landslides generally can be categorized as rock fall and rock slides (rock-planar and rock-wedge slides), as well as shallow translational and rotational soil slides in both native slopes (e.g., cliffs, gulley banks, and steep natural slopes) and anthropogenic slopes (e.g., steep roadway cuts and fills). Earth movements that occurred in native materials (i.e., those not associated with anthropogenic fills or engineered retaining systems) were largely governed by the geology of the material. Rock failures generally involved Miocene flysch units (i.e., a turbidite formation with alternating sandstone and marl layers) and the carbonatic units (i.e., limestones and marly limestones) of the Umbria-Marche Succession. Many of the rock falls occurred in intensely fractured limestone deposits or weak rocks such as breccias, which are locally comprised of moderately cemented travertines and slightly cemented coarse debris. Nearly all soil slides were shallow and occurred in anthropogenic fills or were caused by retaining wall failures. Few of the significant landslide movements that we observed occurred in native slopes.

In early September 2016 and again in early December 2016, the Geotechnical Extreme Events Reconnaissance Association (GEER) organized and mobilized a team of U.S. and Italian researchers including us, the authors, to observe and document the effects of the 2016 Central Italy earthquakes (GEER 2016b, 2017a). Each reconnaissance mission lasted approximately one week. However, the landslides associated with the earthquakes occurred in such frequency and over such a large geographic area, particularly following the M6.5 30 October event, that observing and documenting all of them in detail within a two-week period was not possible. As such, we needed to develop and apply an objective, rapid, and repeatable approach to reconnoiter the largest and most impactful landslides following these events. This approach essentially represented a type of "triage" intended to simultaneously maximize the number of potential landslides visited and the amount of data collected at each site while minimizing the time required to document the earth movements at each site. This type of phased approach is increasingly being implemented and refined by post-earthquake engineering reconnaissance groups including GEER, EERI, and others (e.g., GEER 2016a, Dellow et al. 2017). We similarly incorporated a phased approach that relied on existing landslide mapping, preliminary landslide observations/reports by Italian professionals and authorities, satellite interferometric data, low-altitude aerial imagery collected from unmanned aerial vehicles (UAVs), and traditional manual measurements and documentation to achieve our reconnaissance goals.

This paper describes the phased reconnaissance approach that was applied by us (the Italy-U.S. GEER team) for the rapid documentation of seismic-induced landslides in the days following the Central Italy earthquakes. General observations made from the phased reconnaissance approach are provided, with focus given to three case histories of interest. For brevity, details regarding all of the landslide observations and data are not included in this paper, but are presented in GEER (2016b, 2017a).

LANDSLIDE PHASED RECONNAISSANCE APPROACH

Figure 1 presents a regional vicinity map showing the general location of the three Central Italy earthquakes (Figure 1a), as well as the surface projections of the three

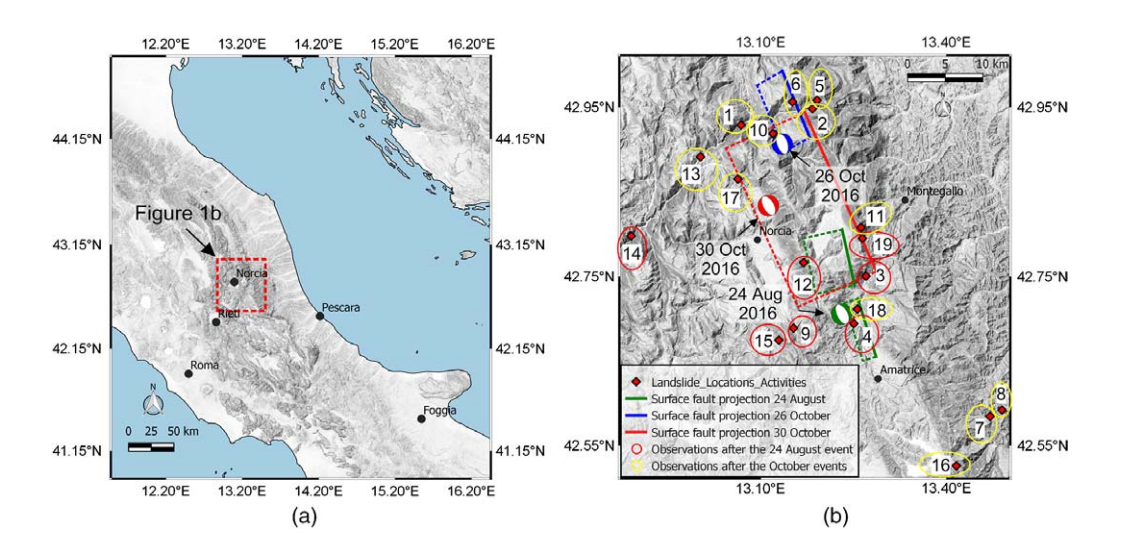


Figure 1. Maps showing (a) the regional vicinity of the earthquakes in Central Italy, and (b) surface projections of the three earthquake rupture planes and associated landslides that were observed. Finite fault models for all three events are from Galadini et al. (2018). Solid lines represent fault traces, dashed lines represent downward-dipping fault planes. The green, blue, and red moment tensors (i.e., "beach balls") are graphical representations of the 24 August, 26 October, and 30 October events, respectively. Numbers in Figure 1b correspond to the sites presented in Table 1.

earthquake rupture planes and corresponding significant landslides that were observed, documented, and/or modeled by our Italy-U.S. GEER team during our September and December 2016 reconnaissance missions (Figure 1b). These landslides and corresponding peak ground acceleration (PGA) estimated values according to Zimmaro et al. (2018) and Galadini et al. (2018) are listed in Table 1. The events circled in red are those observed specifically after the 24 August events, and the events circled in yellow are those observed specifically after the 30 October event. Landslides occurred over an area of approximately 500 km². A summary table listing the landslides shown in Figure 1 is presented in Table 1. Landslides presented in Table 1 are classified according to the terminology of the Hungr et al. (2014) update to the terminology system of Cruden and Varnes (1996).

To reconnoiter the numerous landslides in the region following the initial 24 and 26 August events, an innovative approach different from the manual observation, documentation, and measurement that are commonly associated with geotechnical engineering reconnaissance had to be employed due to the significant size of the affected region, the mountainous terrain, and the limited time available to our team. This approach was again applied and expanded following the 26 and 30 October events. The approach ultimately relied heavily upon select remote sensing methods performed at different scales or coverage areas (i.e., multiscale). While reliance upon a single method of remote sensing limits the captured data to the strength and weaknesses of that particular method, reliance upon multiple remote sensing methods allows the strengths and weaknesses of the various methods to

Table 1. List of landslides that were reconnoitered and documented by the Italy-U.S. GEER team, with estimated PGA values following the three Central Italy earthquakes

- 2				ò				
INO.	Lat.	Long.	M6.1 24 August	M5.9 26 October	M6.5 30 October	Location summary	3D model	Visual obs.
-	42.9290	13.0680	0.22	0.36	0.38	Nera rock slide and avalanche	×	
2	42.9357	13.1901	0.18	0.37	0.40	Monte Bove rock falls	×	
3	42.7506	13.2701	0.48	0.10	0.34	Pescara del Tronto complex landslide	×	×
4	42.6944	13.2503	0.55	0.07	0.40	Accumoli complex landslide	×	×
8	42.9492	13.1880	0.18	0.32	0.35	Valle di Panico rock fall	×	
9	42.9472	13.1436	0.18	0.43	0.43	Valle di Panico rock fall	×	
7	42.5843	13.4708	0.12	0.04	0.12	Cervaro rock fall	×	
∞	42.5919	13.4899	0.11	0.04	0.12	Crognaleto rock fall	×	
6	42.6890	13.1528	0.26	0.10	0.51	Pescia rock fall	×	×
10	42.9188	13.1196	0.21	0.43	0.40	Rock falls along SP-134	×	
11	42.8082	13.2619	0.45	0.13	0.40	Mt. Vettore Massif landslide	×	
12	42.7666	13.1692	0.43	0.18	0.59	Rock fall SP-477	×	
13	42.8913	13.0023	0.17	0.17	0.27	Rock fall SP-209		×
14	42.7980	12.8901	0.10	0.05	0.12	Rock falls between Piedipaterno and Cerreto		×
15	42.6747	13.1290	0.20	0.10	0.40	Disrupted rock slide along SP-746		×
						between Cittareale and Norcia		
16	42.5257	13.4161	60.0	0.03	60.0	Landslide along road near Ortolano-Campotosto		×
17	42.8653	13.0628	0.21	0.35	0.33	Rock falls along SP-476 between Piedivalle		×
						and Preci		
18	42.7114	13.2559	0.56	0.08	0.41	Disrupted rock slide below the Village of Tino		×
19	42.7952	13.2641	0.45	0.12	0.40	SP-477 embankment fill soil slump		×

¹ Numbers for sites are the same as in Figure 1.
² Estimated PGA values developed by Zimmaro et al. (2018) and Galadini et al. (2018) using an assumed average shear wave velocity, V_{S30} of 580 m/s.

complement one another. In this manner, the phased reconnaissance approach resulted in the development of detailed three-dimensional (3-D) scaled models of more than 20 individual landslides from 12 different sites spread over the 500-km² area. The data made available through these models therefore constitute significantly more data than would have otherwise been possible had traditional manual methods of observing and documenting the landslides been solely relied upon.

PRELIMINARY DATA COLLECTION

Following the 24 August event, we first attempted to collect as much preliminary data regarding landslides as possible in the affected Central Italy region. Two initial reports describing observed landslides were of particular use: one report by the Italian Institute for Environmental protection (ISPRA 2016), and another report by the Research Center for Prediction, Prevention and Monitoring of Geological Risks of Sapienza University, provided in the form of a .kmz file (CERI 2016). A third initial report was released by the National Institute for Geophysics and Volcanology (INGV 2016), but provided little information pertaining to landslides. We compared the preliminary landslide observation reports from ISPRA (2016) and CERI (2016) against existing landslide hazard data for the region. Such data were found in two sources: the Inventory of landslide phenomena in Italy (IFFI 2016) and the Plans for Landslide and Flood Risk Management (PAI 2016), which are both developed at the scale of (1:10,000). A thorough comparison of maps extracted from the IFFI inventory and distribution of slope failures/movements observed by CERI (2016) was conducted. While it was observed that most of the landslides documented by CERI (2016) corresponded to locations of known and mapped landslide hazard, some areas with little to no correlation between pre-earthquake mapped landslide hazard and post-earthquake landslide observations were identified (e.g., the villages of Amatrice, Accumoli, Arquata del Tronto, and Pescia). These latter areas were of particular interest and were flagged as possible areas of interest for reconnaissance.

Relatively little published preliminary landslide observation data were available following the 26 October and 30 October events. Fortunately, we already had reasonable understanding of the landslide hazard in the area following the 24 August event. We also relied heavily upon preliminary personal communications from local experts regarding the location of potentially significant landslides to develop a strategy for the December reconnaissance mission.

SATELLITE-BASED DETECTION OF GROUND DEFORMATIONS AND PRELIMINARY SITE SELECTION PROCESS

Recognizing that seismic-induced landslides in the region were extensive and widespread following the 24 August event, our team relied on satellite-based imagery to identify potential areas of interest. In the aftermath of a strong earthquake, satellite-based techniques can be useful to perform rapid detection and mapping of landslides. Recently, Rathje and Franke (2016) described change detection techniques based on pre- and post-event satellite images to detect the spatial distribution of landslides after the 2004 Niigata-ken Chuetsu earthquake. However, satellite-based change detection methods tend to underestimate the size of landslides (Rathje and Carr 2010, Rathje and Franke 2016). Satellite images also can be used to

generate accurate digital elevation models (DEMs; Rathje and Adams 2008). These models can then be used for detecting and monitoring ground and structural deformations. Syntheticaperture radar (SAR) images are often used to achieve this scope. SAR techniques are based on differences in the phase of waves returning to a moving platform (i.e. a satellite). In recent years, SAR-based techniques have been used to identify deformation phenomena such as (1) earthquake-related surface deformations and ruptures (e.g., Fielding et al. 2005, Jo et al. 2010), (2) volcanic eruptions (e.g., Jung et al. 2011, Lee et al. 2013), (3) subsidence (e.g., Choi et al. 2011, Zhang et al. 2012), and (4) massive landslides (e.g., Ausilio and Zimmaro, 2017). Such techniques also can be used for producing rapid post-disaster deformation maps. This is one of the goals of the Advanced Rapid Imaging and Analysis (ARIA) project (http://aria.jpl.nasa.gov/, last accessed 25 July 2017). In recent years, the ARIA project team has released damage proxy maps (DPMs), following main earthquake events globally. The DPMs are produced by comparing interferometric SAR coherence maps from before and after an extreme event (e.g., Fielding et al. 2005, Yun et al. 2011). The effectiveness of DPMs has been recently tested for rapid evaluation of earthquake-induced landslides after the 2015 M7.8 Gorkha earthquake. In particular, Yun et al. (2015) show that the extent of several observed earthquake-related instability phenomena in the Himalayas were well captured by the DPMs. GEER (2017a) and Sextos et al. (2018) also show that DPMs work well in capturing damage patterns in urban areas and historical sites (e.g., the village of Norcia).

Immediately following the M6.1 24 August event, the ARIA project team published a DPM (available at: https://aria-share.jpl.nasa.gov//events/20160824-Italy_EQ/DPM/, last accessed 26 July 2017) for a large portion of the epicentral area. This DPM has a resolution area (extent) of 65×120 kilometers, and was derived using data from the ALOS-2 satellite. A few days after publication of the first DPM, the ARIA project team published a second DPM using data from the COSMO-SkyMed satellite. The latter DPM has a resolution area (extent) of 40×50 kilometers. Figure 2 shows a map of the epicentral area and both DPMs obtained after the 24 August event. The DPMs indicate significantly more potential landslide sites than we could possibly visit during the reconnaissance. As a result, we defined the following scale of priority: (1) size of the landslide, (2) impact to infrastructure, (3) accessibility of the site, and (4) potential for future site characterization. Given the priorities listed above, we initially identified only a few potentially relevant landslide sites based on the DPMs and on available information collected prior to the deployment of the GEER mission: (1) mountain slope north of Cittareale (42.6422 N 13.1634 E), (2) mountain slope north of Pescia (42.6909 N 13.1533 E), (3) eastern slope below the town of Accumoli (42.6941 N 13.2500 E), and (4) the town of Pescara del Tronto (42.7510 N 13.2701 E). These pilot sites also have been used to perform a rapid validation of the effectiveness of DPMs in the area. Main outcomes from this assessment are shown in GEER (2016b) and summarized here. We found that the combination of DPMs and existing mapped landslide locations (e.g., from CERI and ISPRA) proved to be very valuable tools for initial planning of potential landslide locations to be investigated. However, as shown in Figure 2, "hot zones" on DPMs did not always correspond to large landslide features (e.g., the mountain north of Cittareale, which can be classified as a "false positive"). Conversely, a few of the significant landslides we observed did not appear as hot zones on the DPMs ("false negatives"). Similarly, several of the noted CERI landslides also did not appear as hot zones on the DPMs. The DPMs did,

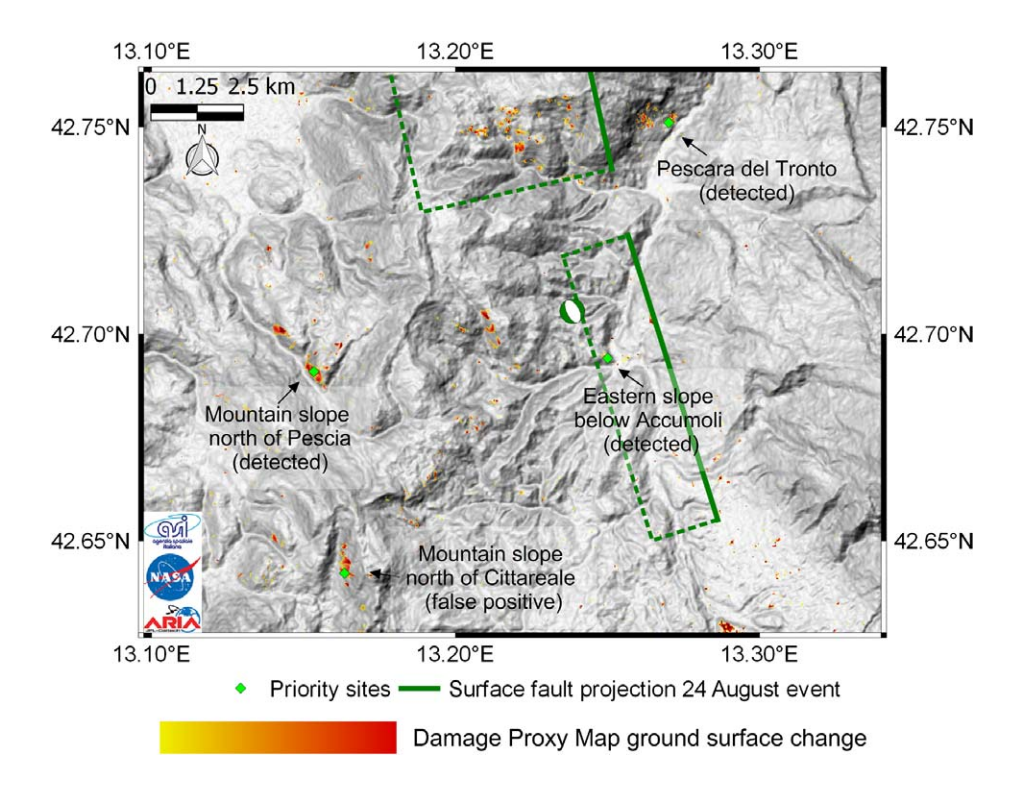


Figure 2. Epicentral area of the M6.1 24 August earthquake along with damage proxy maps of the area produced by the ARIA project. Green moment tensor is the epicenter of the 24 August event. Fault plane of the 30 October event shown in green at the top of the figure.

however, appear to detect most of the significant vertical ground deformations, including widespread structural collapses.

Within a few weeks following the M6.5 30 October event, the ARIA project published a DPM covering a relatively small area near Norcia (https://aria-share.jpl.nasa.gov//events/20161030-Italy_EQ/DPM/, last accessed 25 July 2017). The area affected by seismic-induced landslides following the 30 October event was substantially larger than the area affected following the 24 August event. As a result, we did not use the available DPM in the same manner to define priority sites during the second GEER reconnaissance mission, but instead we used the DPM to identify areas where additional movements may have occurred following the 30 October event.

Overall, we found relatively good agreement between observed landslide features (either from on-site visual inspections or UAV images) and the zones of substantial ground surface change detected by DPMs. However, this outcome is based only on a few pilot sites. As a result, further comparisons between DPMs and observed earthquake-induced landslides are required to further validate this conclusion. We believe that DPMs and similar remote sensing research products readily available following natural disasters can be used to define priority sites for post-disaster reconnaissance missions. Furthermore, when used in combination with

additional GIS information such as topography, vegetation, transportation maps, etc., we believe that DPMs also could be used to distinguish between sites that would benefit from the use of UAVs (e.g., locations where the access may be challenging such as the Nera rock slide site) and sites that would likely be conducive to more traditional inspection approaches such as visual observations. Finally, we believe that DPMs and similar maps also could be used to plan emergency response activities in the aftermath of natural disasters.

USE OF UNMANNED AERIAL VEHICLES FOR LANDSLIDE RECONNAISSANCE

Given the many potential landslide sites indicated by the ARIA project DPMs, a rapid site assessment methodology needed to be implemented to visit and document all of the potentially significant sites during the two relatively brief GEER reconnaissance missions. We elected to use UAVs to image and assess each potential landslide site due to their portability, rapidity in data collection, and superior field of view. While previous GEER reconnaissance missions have incorporated UAVs to varying extents to image one or more sites of interest (e.g., Franke et al. 2017, GEER 2016a, GEER 2017b), the Central Italy GEER missions were unique because the UAV was used as one of the principal data collection tools. The combination of UAV-based low-altitude aerial imagery and targeted terrestrial imagery provided us with a rich dataset of images that ultimately resulted in the development of several two-dimensional (2-D) and 3-D scaled representations of the imaged landslides.

A brief discussion regarding the legalities of operating UAVs following a natural disaster in Italy (and in any country) are warranted. In most developed countries, the operation of UAVs for commercial purposes (including research) is generally heavily regulated, especially following a natural disaster such as an earthquake. However, most regulatory agencies recognize the useful role that UAVs can play following a natural disaster, and systems are typically in place in every country to apply for and obtain authorization to fly. At the time of the reconnaissance missions to Central Italy, the use of UAVs in Italy was subject to Italian Civil Aviation Authority (ENAC) Regulation Issue No. 2. Under this regulation, all UAVs in use had to be registered and operated by an Italian-certified pilot holding an insurance policy. However, given the pressing circumstances following the earthquakes and recognizing the value that low-altitude aerial imagery would provide, the Italian Department of Civil Protection (DPC) issued the Italy-U.S. GEER team an overriding authorization to operate UAVs on a site-by-site basis. The process to obtain this authorization from the DPC required direct communications with administrators within the DPC through our Italian research collaborators. Additionally, implementing the DPC authorization and performing the UAV flights in the field required careful coordination with local military personnel and firefighters, who were generally managing all activities locally on the ground. However, despite DPC authorization, local military and firefighter leaders would not allow us to fly UAVs over several of the most heavily damaged sites, including the village of Amatrice. Fortunately, in the case of landslides, most of the sites of interest were not under lockdown by the military and/or firefighters, and local authorities were generally very eager to assist us in implementing the DPC UAV authorization.

UAV Platforms

Two commercial off-the-shelf (COTS) UAV platforms and one modified/customized COTS UAV platform were used in the Central Italy earthquake reconnaissance.

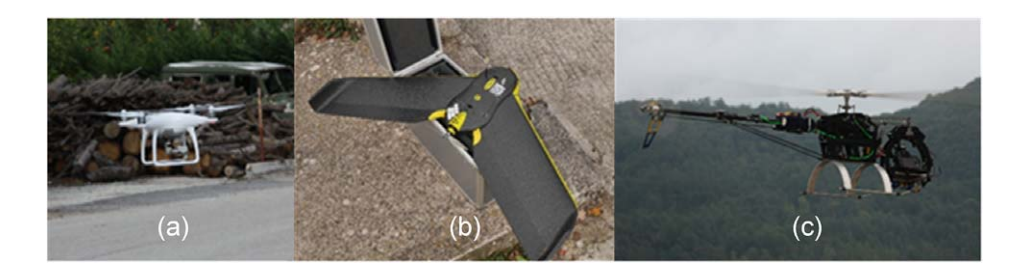


Figure 3. Employed UAV platforms in the Central Italy reconnaissance. (a) DJI Phantom 4, (b) Sensefly eBee, and (c) Align TRex 800e.

These platforms are shown in Figure 3. The majority of the landslide aerial imaging was performed with the DJITM Phantom 4 quadrotor platform (Figure 3a). The Phantom 4 is equipped with a 4K video camera that has a 1/2.3" complimentary metal-oxide-semiconductor (CMOS) sensor, 94-degree field of view, 12.4 MP images, and a focal length of infinity. The platform weighs 1.38 kg, has a maximum flight time of 28 minutes (19 minutes typical), and offers the ability to hover and/or collect imagery from vertical faces such as steep rock cliffs or buildings. The SenseFlyTM eBee fixed wing UAV platform (Figure 3b) was flown over the villages of Accumoli and Pescara del Tronto to image them rapidly. The eBee platform weighs approximately 0.6 kg and can carry a maximum payload of 125 grams. The maximum flight duration is approximately 40 minutes (30 minutes typical), wherein it can image up to 8 square kilometers of ground. The UAV navigates itself using an autopilot and preprogrammed GPS waypoints. The eBee platform used in this study is equipped with a digital camera Canon™ Power Shot S110, which offers a 1/1.7" CMOS sensor, 12 MP images, and a focal length of 5.2 mm. Finally, an AlignTM TRex 800e helicopter UAV platform modified and customized for aerial photography (Figure 3c) was used to image the rock fall at SR-477 due to its capability to maintain stable flight in higher-velocity winds. The modified TRex 800e platform weighs 4.1 kg and incorporates a single propeller that is 1.74 meters in diameter. Due to its size, the TRex 800e can carry a sensor payload of approximately 9 kg. It uses two parallel 6-cell 22.2 volt 8,000 mAh batteries. The TRex 800e used in this study has a 3-axis nose gimbal and uses a NikonTM D750 DSLR camera with 24 MP image resolution, 35.9 × 24.0 CMOS image sensor, and 3-mm fixed focal length lens. The average flight duration of the TRex 800e is relatively short at 12 minutes per battery pair. However, its single, large-diameter propeller provides excellent aerial stability, even with wind gusts exceeding 60 km/hr.

While it may appear questionable that three different UAV platforms were incorporated in the Central Italy reconnaissance, each platform was used for a specific purpose and played a unique and important role in collecting data. The Phantom 4 platform was used primarily to collect high-resolution imagery from sloped or vertical surfaces where vertical control of the platform was necessary. The eBee platform was used primarily to capture nadir images of sites over large areas due to its superior speed and flight endurance. The TRex 800e was used only in one location (the rock fall at SP-477; location #12 in Table 1) because of the heavy winds that were prevalent at that site. It is not possible to identify the optimal UAV platform from this study because each platform was selected based on its intended mission and

environment. Additionally, comparing the performance of different UAV platforms in the reconnaissance was not part of the scope of the research.

A final consideration in the need for multiple UAV platforms in this study is the onboard imaging sensor. Previous studies have demonstrated that Structure from Motion (SfM) models produced from digital single-lens reflex (DSLR) cameras generally are more resolute and accurate than SfM models produced from other smaller point-and-shoot or sport cameras (e.g., Ruggles et al. 2016). However, larger UAV platforms such as the TRex 800 are needed to carry a DSLR camera. In our Central Italy reconnaissance efforts, we decided to rely more on the Phantom 4 and the eBee platforms and their associated cameras because (1) they were more convenient to operate in the field, and (2) the resolution and accuracy provided by the smaller cameras were sufficient for the modeling of post-seismic landslides. Had the objective of our field efforts required more resolute and accurate models (e.g., the modeling of post-seismic structural damage), then we would have sought to implement the TRex 800 with its DSLR camera at more of our sites.

Structure from Motion Photogrammetry Software

One of the most common forms of UAV-based remote sensing involves the use of light-weight optical sensors and a computer vision technique called SfM (Marr and Nishihara 1978, Snavely et al. 2008). For this particular study, commercial SfM software programs *ContextCapture* by Bentley Systems, Inc. (2018) and *Pix4D* by Pix4D SA (2018) were used by the U.S. and Italian researchers, respectively. No comparisons between the products of these two software programs were made, because each program incorporated image sets captured from different UAV platforms and image sensors, which would have confounded any apparent differences between the output from the programs.

The traditional workflow of these and most other commercial and open-source SfM platforms includes:

- Tie Point Extraction: This step usually incorporates the SIFT (scale invariant feature transform) algorithms developed by Lowe (Lowe 2004) or one of its variants to extract from each image a large number of homologous points (i.e., the sparse point cloud).
- Camera Orientation and Calibration: Using camera internal parameters (e.g., focal length, principal point, and distortions), the sparse point cloud is orientated in a local coordinate system (usually connected to the starting reference image) with a relative scale and asset.
- Incorporation of GCPs (ground control points) and CPs (check points): Using a manual survey of several identifiable objects on the ground, a reference system is assigned to the sparse point cloud that enables all of the digital the images to be processed in an efficient and accurate manner, thus enabling the conversion of the sparse point cloud to a global coordinate system.
- Bundle Block Adjustment: Following incorporation of the points, an adjustment is
 performed to the sparse point cloud to minimize location error. This is usually performed with the Levenberg–Marquardt (LM) method, which is an iterative technique that locates a local minimum of a multivariate function expressed as the sum of
 squares of several nonlinear, real-valued functions.

- Dense Point Cloud Generation: Once the sparse point cloud has been developed, dense point cloud generation is initiated using the sparse point cloud as a "lattice" for the dense cloud. The techniques and algorithms used to develop the dense point cloud vary. However, most of these techniques and algorithms incorporate some variant of the semi global matching approach proposed by Hirschmüller (2005, 2008).
- Output Development: The final 3-D dense point cloud enables the development of products such as a DSM (digital surface model), DEM, Orthophoto, and 3-D mesh textured model.

The accuracy of the final SfM products from sites where surveyed GCPs were performed was checked on several CPs during the Bundle Block Adjustment, with the resulting RMS (root mean square) error of the evaluated CPs falling under 5 cm at each site. These observed results correspond well with the SfM model RMS error range of 2 cm to 5 cm reported by Turner et al. (2015). We can therefore assume mean accuracy (horizontal and/or vertical) of 2 cm to 5 cm in the SfM 3-D point cloud and meshed DSM models at these sites. Other sites where surveyed GCPs and CPs were not performed due to limited surveying resources yielded less desirable accuracies (horizontal and vertical) of 1.3 meters or better based on our comparisons with high-resolution DEMs. Ultimately, UAV-based DSMs of post-earthquake damage such as those created through these reconnaissance missions have been used by previous researchers to study and/or measure the displacements of individual landslides over a given timeframe of interest (e.g., Niethammer et al. 2012, Stumpf et al. 2013, Lucieer et al. 2014, Ruggles et al. 2016), as well as the effects of soil liquefaction (Franke et al. 2017) and seismic-induced landslides (Zekkos et al. 2017).

Resulting 3-D Models and Orthophotos

For the landslide sites that were imaged with UAVs, we developed orthophotos and/or 3-D mesh textured models in the weeks following each GEER reconnaissance mission. A summary of the sites for which 3-D mesh textured models are available is included in Table 1. Orthophotos of landslides without villages were developed with ContextCapture. Orthophotos were developed with Pix4D for the imaged landslides in the villages of Pescara del Tronto and Accumoli for future photogrammetric analysis of structural damage. For example, Figure 4a presents a split image of Pescara del Tronto and its landslides following the 24 August event, with one portion demonstrated as a DEM raster (left) and the other portion as an orthophoto (right). Figure 4b presents an orthophoto of the same village following the 30 October event. Optical image correlation methods could then be performed using such orthophotos to potentially identify horizontal deformations of the landslides (e.g., Rathje et al. 2006, Martin and Rathje 2014). All 3-D mesh textured models developed from ContextCapture can be viewed and explored online with any standard Internet browser using the free Acute3D Web Viewer add-in by Bentley Systems, Inc. (2018), which allows for basic retrieval of latitude, longitude, and elevation information from the model, as well as basic linear measurement between two points. Links to the available Central Italy 3-D landslide and rock fall models are at http://prismweb.groups.et.byu.net/ gallery2/2016%20Central%20Italy%20Earthquakes/. In the case of landslides, the 3-D models can be used to measure strike and dip of rock angles and bedding planes for geostructural

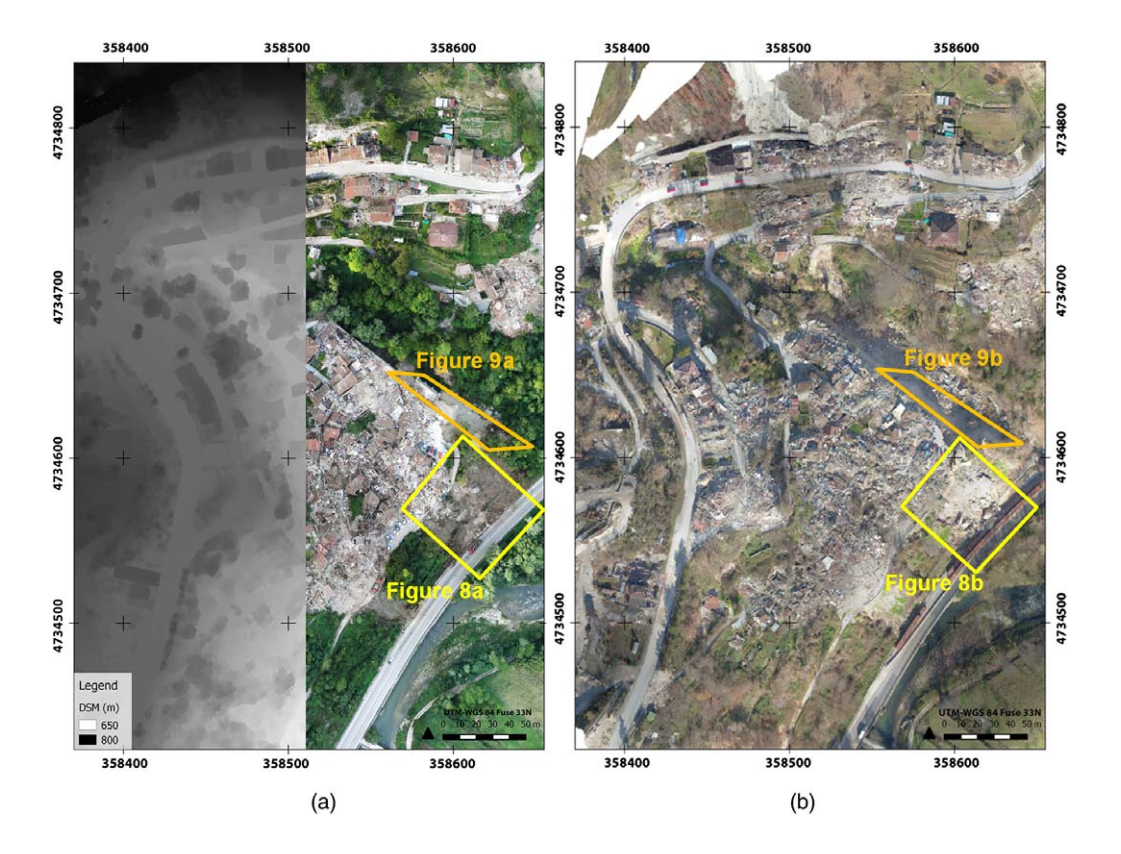


Figure 4. Output of the UAV-based remote sensing at the landslides in the village of Pescara del Tronto showing (a) split DEM and orthophoto of the village following the 24 August event, and (b) orthophoto of the village following the 30 October event.

analysis of rock surfaces, dimensions and runout distances of boulders, and volume estimates of scarps and talus cones (e.g., Franke et al. 2018).

VISUAL INSPECTION AND OBSERVATION

In addition to the UAV aerial imaging described above, we performed manual inspection and documentation of landslides where possible at sites that were accessible from local roads. In some cases (such as Mt. Bove), extreme terrain made rapid visual inspection impossible. For these landslides, only UAV-based inspection was possible. Manual inspection was performed using conventional geologists' tools: rock hammers, compass, clinometer, scale, measuring tape, and total station. When arriving at a new landslide location, an initial visual survey of the area was performed by traversing the fall or slide area. Once the extents of the source and/or accumulation area of the slide were established, we began mapping the landslide. GPS coordinates of the slide or fall were taken at key points, most often along an impacted or adjacent roadway, so that good accuracy could be obtained from multiple satellites in the horizon. In many cases, heavy vegetation, cliffs, or steep hillsides prevented good GPS location accuracy on the slide mass itself.

For each manually inspected site, we measured key landslide dimensions of the slide such as width, length, scarp height, and slope inclination. Detailed notes were taken on the local geology, observed groundwater and seepage conditions, anthropogenic activity in the area, and constituent materials of the slide mass. For most of the landslides, lateral deformations were small enough that hand measurements of scarp height and lateral movement were possible. For rock falls, we attempted to ascend slopes to rock source faces, though in many cases were unable to mount such expeditions in the limited time available. Total stations were used to measure the key dimensions of the rock fall source such as width and height. Slope inclination below the rock source was either measured or estimated. Detailed notes were taken on the local geology, observed groundwater and seepage conditions, anthropogenic activity in the area, and constituent materials of the rock fall. If an inspection of the rock source was performed, rock strength was inferred with a geologic hammer. Infill material was evaluated along with joint width, spacing, weathering, and bedding. For most of the rock falls, lateral and vertical distances of rollout were too large to measure by hand, and distances were estimated. Boulder fragments were inspected in the same detail as the rock source, with measurements of boulder size.

TERRESTRIAL LASER SCANNING

We used terrestrial LiDAR at select landslide locations during the reconnaissance mission. Terrestrial LiDAR point cloud models proved to be useful intermediaries between UAV and manual inspections. LiDAR can be highly accurate and cover large areas, but shadows cast by changes in slopes and hillsides can block critical areas from view. This requires additional LiDAR surveys from alternate directions or fusing with a UAV-based SfM point cloud model. LiDAR was observed to be much slower than UAV-based inspections, but was still much faster than manual inspection of large areas. Additionally, its accuracy is generally superior to UAV-based remote sensing.

SIGNIFICANT OBSERVATIONS RESULTING FROM THE PHASED RECONNAISSANCE APPROACH

EARTHQUAKE SEQUENCE AND DAMAGE ACCUMULATION

The phased reconnaissance approach allowed us to observe that landslide deformations varied considerably between events during the 2016 earthquake sequence. In fact, some areas that showed very little deformation after the 24 and 26 August events showed large deformations after the 26 October or 30 October events. The largest deformations generally correlated with the largest of the events, the 30 October event. This observation makes sense because earthquake magnitude is generally proportional to measured ground motion parameters such as PGA, peak ground velocity, I_a, and significant duration. However, as Table 1 indicates, some of the landslides that moved significantly in October likely experienced smaller PGAs than in August due to their greater distance from the seismic rupture. Recording stations in most areas showed a longer bracketed duration for the M6.5 event than the M6.1 event (see Table 2 for an example of one such recording station in the high-damage area south of the rupture plane for the seismic series). Table 2 shows a summary of ground motion recording details for the entire sequence at the Amatrice recording station (AMT). This station near the heavily damaged village of Amatrice showed higher peak east-west horizontal accelerations

Table 2. Earthquake sequence ground motion summary for one recording station (AMT) located near the landslides at the villages of Pescara del Tronto and Accumoli

Date and magnitude	PHGA1 ¹ (g)	PHGA2 ¹ (g)	PHGV1 ² (cm/s)	PHGV2 ² (cm/s)	CAV ³ (cm/s)	I _a ³ (m/s)	Bracketed duration (s) ³
24 August 2016 M 6.0	0.88	0.38	45.0	41.5	739	1.89	9.47
24 August 2016 M5.3	0.11	0.10	3.95	5.1	159.5	0.06	2.47
26 August 2016 M4.8	0.33	0.34	7.70	11.0	193.3	0.26	2.17
26 October 2016 M5.4	0.09	0.06	3.81	3.10	121.0	0.04	1.01
26 October 2016 M5.9	0.09	0.06	5.44	3.47	193.9	0.06	1.14
30 October 2016 M6.5	0.53	0.40	37.9	33.5	833	1.57	11.37

¹ Orthogonal peak horizontal ground accelerations (E-W, N-S directions).

in the M6.1 event along with higher peak horizontal ground velocity (PHGV); however, the M6.5 event was more damaging to the village and caused more landslides in the surrounding area with higher cumulative absolute velocity (CAV), Ia and higher accelerations in the northsouth direction. Such locations include the villages of Pescara del Tronto, Accumoli, and Tino. These villages appeared to have experienced more landslides during the longer duration 30 October event than during the more intense 24 August event. Recording stations in other locations show similar or different trends depending on local site effects and geometric effects (hanging wall versus foot wall, etc). Subsequent analysis has identified two primary contributing factors to the observed landslide patterns and sequencing: 1) differences in ground motion duration and intensity from the different events due to a combination of event magnitude, siteto-source distance, local site effects, and geometric effects, but with the M6.5 event consistently producing the largest recorded CAV and I_a values; and 2) the accumulation of incremental damage from all of the preceding earthquakes resulting in large soil and rock mass movements during the M6.5 30 October event. Because of the paucity of high-quality ground motion recordings from the most affected areas in the Central Italy earthquake sequence, it is currently not possible for us to determine which of these two suspected factors (i.e., differences in ground motions from individual events versus incremental damage) contributed most to the observed landslide distribution or individual landslide behavior.

CASE HISTORIES OF INTEREST

Three landslides in Table 1 that are considered significant based on their size, contribution to our current understanding, and/or apparent impact to surrounding infrastructure will now be briefly described. Additional studies are currently underway to investigate these significant landslides further using the data collected from the phased reconnaissance approach. Information regarding the other landslides in Table 1 are described in greater detail in GEER (2016b, 2017a).

Nera Rock Fall

A rock fall triggered by the 30 October earthquake on the left bank of the Nera River affected a state highway route (SR209) connecting Visso to Terni in the Umbria Region and

² Peak horizontal ground velocity (E-W, N-S directions).

³ Maximum of E-W or N-S direction.

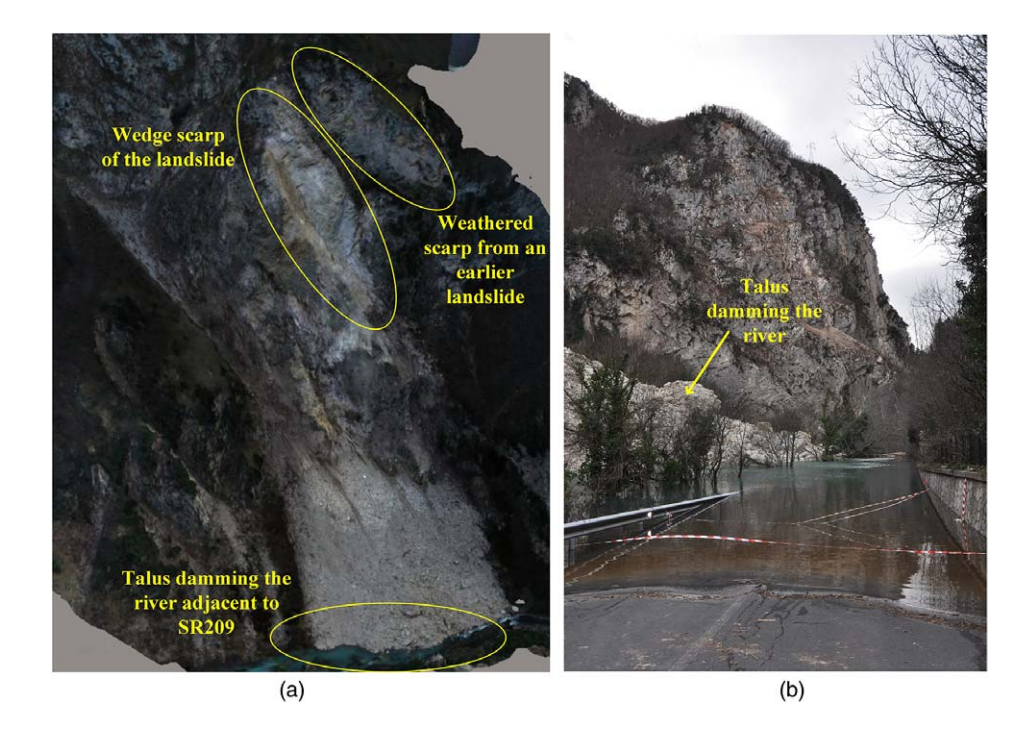


Figure 5. Nera landslide: (a) image taken from the UAV-based 3-D mesh model of the landslide; and (b) photograph of the dammed Nera River blocking SR209.

dammed the adjacent Nera River. This rock fall is significant because of its impact to local infrastructure and recovery efforts, and because it does not appear on any of the current IFFI or PAI landslide catalogs. Images of the 3-D model of the Nera rock fall and a photograph of the dammed river are presented in Figure 5.

Analysis of the landslide site using the UAV-based 3-D DSM suggests that the total volume of talus at base of the slope at the time of the UAV flight in December was between 65,000 m³ and 70,000 m³. This volume was calculated by differencing the UAV-based 3-D DSM and a pre-earthquake digital terrain model developed from aerial LiDAR that was captured by the Italian Ministry for Environment and Cultural Heritage in 2013. The estimate of the volume of the failed rock wedge on the slope varies according to the hypothesized shape of the original cliff surface. Inspection of the UAV-based 3-D DSM suggests that the original cliff surface was likely formed by discontinuities belonging to the current delimiting wedge, thus forming a prismatic shape for the failed rock mass. Assuming this prismatic shape, the volume of rock that fell is computed to be approximately 32,000 m³. Assuming a factor of 1.4 to account for the increased porosity in the shattered talus, which is a common factor used by engineering geologists, the total volume of fragmented rock from the Nera rock fall is approximately 45,000 m³, which falls within the standard of error of the volume estimate provided by Romeo et al. (2017), who performed laser scan-based measurements at the landslide. The difference between the total volume of the deposit and the estimated volume associated with the failed wedge (i.e., 20,000 m³ to 25,000 m³) can be attributed to landslides that

occurred prior to the 30 October event. For example, one such landslide could be from the large, weathered scarp located above the new scarp and that is apparent in the UAV-based images and 3-D DSMs (see Figure 5a). More detailed analysis of the Nera landslide and demonstrated use of its UAV-based 3-D DSM is presented in Franke et al. (2018).

Based on our preliminary assessment, an initial rock fall appears to have triggered a larger rock wedge slide in the sedimentary rocks of the Umbria-Marche stratigraphic sequence, an early Jurassic to Eocene age formation. The Nera River Valley is formed on an anticline fold that was dislocated and uplifted during the Plio-Quaternary era. The steepness of the slopes and the inherited fracture network affect slope stability in the area. The rock fall involved a thinly bedded limestone formation (*Maiolica*) deposited in basin facies of the Umbria-Marche sequence per data available from the provinces of Umbria and Marche (e.g., Regione Umbria 2014). The structural setting of the slope is complex, with an eroded-hinge anticline. On the west flank, a relevant extensional master fault is present, dipping towards the southeast.

Crognaleto Rock Falls

The second significant landslide site that we observed was comprised of two separate but adjacent rock falls located near the village of Crognaleto (landslides Numbers 7 and 8 in Table 1). These rock falls are considered significant for two reasons: (1) the data captured from the phased reconnaissance approach allows us to measure very accurate runout distances and boulder volumes, which can be used to improve and/or validate rock fall prediction models in future studies; and (2) the known timing of the rock falls combined with our best estimates of ground motion parameters at the sites during the three earthquake events may help us better understand through future studies how rock falls can be triggered from repeated seismic events in close proximity to each other. We visited the two sites in the Crognaleto Municipality at the request of the Highway Department of Teramo Province, who observed large rock falls near the villages of Cervaro and Crognaleto along roads SP-45a and SP-45e in the northeastern foothills of the Gran Sasso Massif. Figure 1 shows the two rock falls as Sites 7 and 8. No evidence of major rock falls was noticed in the subject region after the 24 August and 26 October events. Nevertheless, these earlier events may have loosened the rock mass, especially through cyclic degradation of the strength at the sandstone–mudstone contacts and by decreasing block interlocking. Similarly, there is no clear evidence of rock falls caused by the 2009 L'Aquila seismic sequence, which was comprised of four normal faulting events ranging in size from M4.4 to M6.3 and that occurred approximately 29 km to the south. However, the finding of large, old blocks at both sites indicates the two slopes have experienced past rock falls. Rainfall data recorded at the Crognaleto station showed that both daily rainfall and rainfall accumulated over one and two weeks were not appreciable prior to the 30 October event. 3-D model images of these rock fall sites are presented in Figure 6.

Both rock falls affected ledges formed by thick sandstone layers of the Laga Formation, a turbidite formation consisting of alternating sandstone and marl/mudstone layers (Bigi et al. 2013). The formation, characterized by a regular structural setting with sub-horizontal or gently dipping bedding, outcrops extensively in the area, where it forms high and steep slopes. The sandstone (S) to marl (M) ratio and bedding joint spacing are highly variable, depending on their paleo-environmental location. At both the Crognaleto and Cervaro sites,

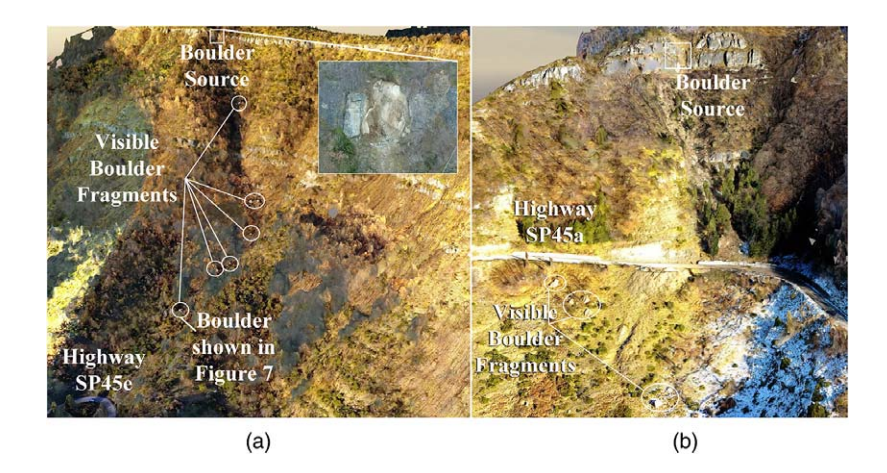


Figure 6. 3-D models of the two rock falls in the area of the villages of Cervaro and Crognaleto in Teramo Province: (a) Site 7 along SP-45e, near the Village of Cervaro; and (b) site 8 along SP-45a, near the Village of Crognaleto.

sequences of thin mudstone layers and sandstone layers up to 9 m thick are frequent. Observations conducted on several ledges indicate that sandstone layers are crossed by vertical joints of tectonic origin normal to the slope face and are spaced up to 8–9 m. Persistence of vertical joints is sufficient to crosscut the whole rock layer. As a consequence, block volume can easily reach tens of cubic meters.

The source of the observed rock falls at these two sites is a 3.5-m- to 8-m-thick sandstone layer that sits at the top of the slope like a rim (see Figure 6). Several other smaller source areas were identified on the mid-slope rock faces. However, UAV-based data indicate that most of the boulders that stopped just upslope from the roads came from the rim-rock exposure at the top of the slope. Just below the rim-rock face, the slope is 30° to 35° until about mid-slope above the SP-45a and SP-45e roadways, where other large sandstone layers produce 3-m- to 12-m-high vertical scarps. Below these scarps, the slope flattens to 18° to 20°. Below the roadways, the slope continues at 18° to 20°. Below the source zone, rock blocks followed drainage paths and stopped just above or below the roadways.

Due to the steep terrain and the long runout distances, we relied primarily on UAV and LiDAR to collect data. We carefully examined the larger boulder fragments that reached the roadways. The UAV-based 3-D models of both rock fall sites presented in Figure 6 measure boulder sources that are 250 m above SP-45e and 150 m above SP-45a at Cervaro and Crognaleto, respectively. The runout distance covered by the largest boulder fragments at Cervaro was measured to be 0.5 km, while the maximum runout distance at Crognaleto was measured at 260 m. At Cervaro, the volume of the detached block is estimated from UAV-based 3-D models and manual measurements to be 55 m³. During runout, the block appears to have progressively fragmented. This is witnessed by littering of the rock fall path with boulder fragments, some as large as 2 m in diameter. The largest boulder fragment that we measured at Cervaro (circled in Figure 6a, and shown in Figure 7) was 4 m in diameter, while the largest boulder fragment observed at Crognaleto was 3 m in diameter. The fragmented boulders



Figure 7. Largest boulder fragment observed at the Cervaro Rock Fall site (circled in Figure 6a).

along the runout path showed fresh fractures and little signs of weathering, thus suggesting that these fragments were not existing blocks on the slope that were reactivated by the earth-quake or another falling boulder. Furthermore, the corridor of trampled trees at the Cervaro site was measured in both the field and the UAV-based 3-D DSM to be more than 12 m wide, suggesting a single, 12-meter-wide boulder that inflicted the damage before it fractured into smaller boulders. The actual largest boulder diameter at Crognaleto is unknown, because the largest boulders landed on the SP-45a highway after having broken the retaining wall at the backslope. These largest boulders were blasted and removed by road repair crews prior to our arrival.

Table 1 indicates that the computed PGAs in the area of Cervaro and Crognaleto were likely similar between the 24 August and 30 October events (Zimmaro et al. 2018). No significant damage was observed by locals following the 26 October event due to the very small ground motions in the area. To evaluate why the rock falls were triggered during the 30 October M6.5 event, the ground motion recording information from the three closest ground motion recording stations with similar site conditions was studied for the 24 August and 30 October events. Ground motion parameters from these three stations are presented in Table 3 (Stations TERO, MCS, and PCB are all within 12-km distance of the subject locations, while the other stations are within 50 km). Recorded ground motions from the 26 October event were very small and are therefore not included in Table 3. While PHGAs were similar between the two events, the PHGV, cumulative absolute velocity, and Arias intensity were much higher in the 30 October event. These rock falls therefore appear to be cases in which velocity and cumulative energy had a greater effect on triggering rock slope instabilities than peak horizontal ground accelerations. Ongoing studies are continuing to investigate and test this observation further.

Event	Stations: V_{S30} (m/s)	TERO 660	MSC 540	PCB 366	SPM 1000	CSC 698	NOR 687
August	PHGA (g)	0.09	0.05	0.13	0.07	0.06	0.19
M 6.1	PHGV (cm/s)	4.29	1.43	5.49	3.02	2.01	21.09
NS	I_a (m/s)	0.08	0.02	0.21	0.05	0.03	0.34
	CAV (cm/s)	236.15	75.41	194.06	206.99	132.33	504.67
August	PHGA (g)	0.06	0.05	0.12	0.07	0.05	0.21
M 6.1	PHGV (cm/s)	3.15	0.93	2.60	2.36	2.71	27.15
EW	I_a (m/s)	0.05	0.01	0.07	0.05	0.03	0.56
	CAV (cm/s)	203.48	65.13	131.84	205.96	119.48	593.93
October	PHGA (g)	0.12	0.10	0.25	0.08	0.16	0.29
M6.5	PHGV (cm/s)	7.04	8.42	9.62	4.91	13.64	48.03
NS	I_a (m/s)	0.21	0.11	0.37	0.13	0.37	1.43
	CAV (cm/s)	392.42	296.71	450.71	354.59	493.03	1,115.53
October	PHGA (g)	0.09	0.10	0.15	0.10	0.17	0.31
M 6.5 EW	PHGV (cm/s)	5.32	9.03	8.46	6.78	13.82	57.22
	I _a (m/s)	0.10	0.10	0.13	0.18	0.31	2.90
	CAV (cm/s)	311.55	285.83	293.94	415.15	455.87	1,607.02

Table 3. Select ground motion recording station record summaries south of the Mt. Vettore Fault

Village of Pescara del Tronto

The final significant site that will be summarized are the numerous landslides and retaining wall failures that occurred beneath and in the village of Pescara del Tronto. These events are considered significant for two principal reasons: (1) the impacts that the landslides and wall failures had on the surrounding infrastructure, and (2) the observed timing and sequential nature of the failures with the three earthquake events. Following the 24 August event, early observations by Italian investigators reported significant soil and structural deformations in Pescara del Tronto (Site 3 in Figure 1 and Table 1). However, at the time of our arrival, the village was evacuated and guarded by military and firefighting personnel. Upon gaining authorization to enter the town for reconnaissance purposes, we were allowed only two hours to perform all reconnaissance activities under close supervision from a team of firefighters. Due to the size of the village, the level and extent of the damage, and limited time frame granted to the team, the Phantom 4 UAV was used to image the entire village. In the second GEER investigation in December following the 26 and 30 October events, all structures in the village had collapsed, and obtaining reconnaissance authorization from the firefighters and the military was easier. However, manual inspection of the damage was severely limited due to safety concerns, so the Phantom 4 UAV was again used to image the entire village.

Investigation of the resulting 3-D models and orthophotos of Pescara del Tronto from SfM computer vision revealed numerous shallow debris slides and retaining wall failures throughout the village following the 24 August event. These debris slides and wall failures

only worsened following the October events. Two of the most significant deformations will be described here; descriptions of the remaining observed deformations are presented in GEER (2016b, 2017a). The first is the largest debris slide that was observed on the east slope directly below Pescara del Tronto (directly above Highway SS4). 3-D model images of this debris slide following the 24 August and 30 October events are presented in Figure 8. This debris slide was approximately 75 meters wide by 30 meters high. On the exposed slide surface, UAV images contributed to ascertain that the foot of the slope is formed by sandstones of the Miocene flysch bedrock and that it is overlain by a fluvio-lacustrine sequence including sandy-silty sediments and travertines. UAV models also clarified that the fluviolacustrine sequence had been involved in old landslides, as it is demonstrated by the rotation of large travertine blocks not involved in the failure. The debris slide itself was initially quite shallow, with only the upper meter or less of soil sliding downslope. The debris slide damaged and/or undercut retaining wall structures surrounding the city, leaving portions of the overlying city dangerously susceptible to collapse. Two large limestone boulders, remnants of an old slide, remained exposed along the slope above Highway SS-4, and it was not immediately clear their safety margin against sliding/toppling. No significant deformations in the village were observed by firefighters or military personnel following the smaller 26 October event. However, ground motions from the larger 30 October event dislodged the two large limestone boulders and other travertine blocks, bringing them down the slope towards Highway SS4 (Figure 8b). Fortunately, a makeshift barrier comprising cargo shipping containers had been placed along the highway by Italian authorities, thus preventing the large boulders from running out onto the highway.

The second deformation, and one of the more dramatic geotechnical failures that was observed by our team following the Central Italy earthquake sequence, is the sequential collapse of the massive 25-meter-high masonry retaining walls located adjacent to the creek and gulley below the village. Figure 9 presents 3-D model images of the retaining walls following the 24 August and 30 October events. Damage to the walls following the 24 August event (Figure 9a) was initially limited to the lower corner of the village, directly above Highway SS4. Additional shaking from the 26 August and 30 October events was sufficient to collapse



Figure 8. 3-D mesh model images of the largest observed debris slide below the village of Pescara del Tronto following the (a) 24 August and (b) 30 October events.



Figure 9. 3-D mesh model images of the debris slide and retaining wall collapse below the village of Pescara del Tronto following the (a) 24 August and (b) 30 October events.

the remaining walls, all engineered backfill, and any overlying structures, thus leaving behind native cut slopes at a dip angle of 53 degrees (Figure 9b).

LESSONS LEARNED AND CONCLUSIONS

The phased reconnaissance approach that was applied by the GEER team to the reconnaissance of landslides induced by the Central Italy earthquake sequence is considered a success. The approach greatly increased the number of landslide sites that could be visited and documented by GEER researchers over the two-week period that they were in the field. Furthermore, the approach enabled the development of scaled 3-D landslide models on a scale never before seen in a post-earthquake reconnaissance effort. These models allow researchers who were not present in the field to study these sites as if they were present, thus vastly increasing the impact of the reconnaissance effort. The 3-D models and orthophotos developed from these reconnaissance efforts continue to provide benefit to researchers attempting to better understand the mechanisms that cause seismic-induced landslides and to improve our ability to predict their occurrence and associated movements.

Several valuable lessons were learned from the application of this phased approach in Central Italy:

- No one method of remote sensing can obtain the coverage and accuracy that is typically desired in a post-earthquake reconnaissance effort. An ideal phased approach first relies upon broad, coarse remote sensing methods such as satellite-based interferometry or optical image correlation to identify areas where significant deformations may have occurred. More localized and accurate remote sensing methods such as UAV-based SfM and/or terrestrial LiDAR are then deployed to collect data from potential sites of interest.
- When implemented in a GIS framework with preliminary landslide observations, satellite photographs of the earth, and maps of existing active landslides, the DPMs proved most valuable to the GEER team for selecting potential sites of interest to reconnoiter. However, both false positives and false negatives were observed with the maps, and thus they should not be relied upon as a standalone tool for quantifying ground deformations.
- 3. The incorporation of surveyed GCPs and CPs in the UAV-based reconnaissance of landslide sites greatly increases the accuracy of the resulting products. For example, accuracy assessments of the Central Italy 3-D models show that the accuracies of the models where surveyed GCPs and CPs were performed and incorporated into the SfM processing were generally smaller than 5 cm. However, 3-D models that were developed from images without GCPs and CPs, but instead relied upon the GPS equipment onboard the UAV, generally were observed to have model accuracies within 1.3 m based on comparisons between manual tape measurements in the field and measurements in the point clouds and DSMs. Therefore, careful consideration must be given regarding the desired level of accuracy from the resulting 3-D models and associated effort in the field.
- 4. Once the UAV is in the air, the onboard camera is the factor that seems to govern the quality of the data that are collected. Other factors such as UAV speed and altitude can be adjusted mid-flight as necessary, but only minimal adjustments can be made to improve camera performance. In general, DSLR or DSLR-equivalent cameras (e.g., mirrorless DSLR) are preferred over traditional point-and-shoot cameras, but they require larger UAV platforms to carry them.

Two specific recommendations can be made for improved implementation of the phased reconnaissance approach described in this paper for future reconnaissance efforts, namely:

- The Central Italy landslide reconnaissance effort was much more efficient and effective during the December reconnaissance when an initial "scouting" team of researchers (in this case, a team of local Italian researchers) first located potential landslide sites of interest. Shortly thereafter, a second "imaging" and data collection team of researchers was dispatched to carefully reconnoiter all the identified landslide sites of interest. Future reconnaissance efforts should implement a similar staged reconnaissance.
- 2. The incorporation of one or more team(s) of surveyors in a reconnaissance effort can greatly increase the efficiency of field activities and the accuracy of remote sensing products. This team can move slightly ahead of the imaging team, preparing beforehand each site with surveyed GCPs and CPs.

While traditional manual observation will always be necessary in the reconnaissance of land-slides, the results of this study have demonstrated that future efforts could incorporate a phased reconnaissance approach as described in this paper, and rely even more upon UAV-based SfM and terrestrial LiDAR remote sensing methods. Future reconnaissance teams should send teams of manual observers to perform traditional measurements at landslide sites in a very selective manner, visiting only those sites where such activities are deemed most valuable and essential. The possibility of each reconnaissance team member carrying and incorporating a small UAV platform is not likely in the current regulatory environment because of the certifications that are typically required to operate UAVs in a commercial setting. If such regulations are relaxed for researchers in the future, then it will be very feasible and advantageous for each member of a reconnaissance team to carry and operate (where needed) a small UAV platform. Continuous advances in efficiency and convenience of SfM processing and UAV operation software are increasingly making these tools available to a larger set of the population.

ACKNOWLEDGMENTS

The GEER Association is supported by the National Science Foundation (NSF) through the Geotechnical Engineering Program under Grant Number CMMI-1266418. Any opinions, findings, and conclusions or recommendations expressed in this material are those of the authors and do not necessarily reflect the views of the NSF. The GEER Association is made possible by the vision and support of the NSF Geotechnical Engineering Program Directors: Richard Fragaszy and the late Cliff Astill. GEER members also donate their time, talent, and resources to collect time-sensitive field observations of the effects of extreme events. This work was also partially supported by the Center for Unmanned Aircraft Systems (C-UAS), a National Science Foundation Industry/University Cooperative Research Center (I/UCRC) under NSF Award Number CNS-1650547, along with significant contributions from C-UAS industry members. UAV flight permits and access to several landslide areas were obtained thanks to the help of Paola Pagliara and Paola Bertuccioli of Dipartimento della protezione civile (DPC). Thanks are due to Monica Di Mattia and Dario Melozzi of the Highway Dept. of Teramo Provence for their assistance during reconnaissance operations at Cervaro and Crognaleto and to Giuseppe Riccioni (Ussita Municipality) and Roberto Cantoni and Raffaele Sorriento (Corpo Nazionale dei Vigili del Fuoco), who allowed the survey of the northern flank of Monte Bove and Valle di Panico. Finally, we acknowledge the excellent work by the graduate students and faculty collaborators in performing the SfM processing and developing the 3-D models discussed in this study. These individuals include Benjamin Barrett, Brigette Ostrum, Jenny Blonquist, Jacob Wilcock, and John Hedengren. We offer a special thanks to the UAV operator (undergraduate student researcher) Brandon Reimschiissel for his efforts in collecting the data from this study. We also acknowledge the work and efforts of the entire GEER Central Italy team.

REFERENCES

Ausilio, E., and Zimmaro, P., 2017. Landslide characterization using a multidisciplinary approach, *Measurement* **104**, 294–301.

Bentley Systems, Inc., 2018. *ContextCapture*, software, available at https://www.bentley.com/en/products/brands/contextcapture.

Bigi, S., Conti, A., Casero, P., Ruggiero, L., Recanati, R., and Lipparini, L., 2013. Geological model of the central Periadriatic basin (Apennines, Italy), *Marine and Petroleum Geology* 42, 107–121.

Boccardo, P., Chiabrando, F., Dutto, F., Tonolo, F. G., and Lingua, A., 2015. UAV deployment exercise for mapping purposes: Evaluation of emergency response applications, *Sensors* **15**, 15717–15737.

- Brown, C. B., 1971. Close-range camera calibration, *Photogrammetric Engineering* 37, 855–866.
- Centro Di Ricerca Previsione, Prevenzione e Controllo Dei Rischi Geologici (CERI) Working Group, Martino, S., Caporossi, P., Della Seta, M., Esposito, C., Fantini, A., Fiorucci, M., Iannucci, R., Marmoni, G. M., Mazzanti, P., Moretto, S., Rivellino, S., Romeo, R. W., Sarandrea, P., Troiani, F., and Varone, C., 2016. Sisma Amatrice Effetti- Interazione rete infrastrutturale, available at http://www.ceri.uniroma1.it/ (last accessed 22 March 2017).
- Choi, J.-K., Won, J.-S., Lee, S., Kim, S.-W., Kim, K.-D., and Jung, H.-S., 2011. Integration of GIS and SAR interferometry for a coal mine subsidence hazard map in Taebaek, Korea, *International Journal of Remote Sensing* 32, 8161–8181.
- Cruden, D. M., and Varnes, D. J., 1996. Landslide types and processes, in *Landslides Investigation and Mitigation, Special Report 247* (A. K. Turner and R. L. Schuster, eds.), Transportation Research Board, U.S. National Research Council, Washington, D.C., 36–75.
- Dellow, S., Massey, C., Cox, S, Archibald, G., Begg, J., Bruce, Z., Carey, J., Davidson, J., Della Pasqua, F., Glassey, P., Hill, M., Jones, K., Lyndesell, B., Lukovic, B., McColl, S., Rattenbury, M., Read, S., Rosser, B., Singeisen, C., Townsend, D., Villamor, P., Villeneuve, M., Godt, J., Jibson, R., Allstadt, K., Rengers, F., Wartman, J., Rathje, E., Sitar, N., Athanasopoulos-Zekkos, A., Manousakis, J., and Little, M., 2017. Landslides caused by the Mw7.8 Kaikoura earthquake and the immediate response, *Bulletin of the New Zealand Society for Earthquake Engineering* **50**(2), 106–116.
- Fielding, E. J., Talebian, M., Rosen, P. A., Nazari, H., Jackson, A., Ghorashi, M., and Walker, R., 2005. Surface ruptures and building damage of the 2003 Bam, Iran, earthquake mapped by satellite synthetic aperture radar interferometric correlation, *Journal of Geophysical Research* 110, B03302.
- Franke, K. W., Kayen, R. E., Santo, A., Chiabrando, F., Blonquist, J., and Barrett, B., 2018. UAV-based reconnaissance and analysis of a large seismic-induced landslide in central Italy, 11th National Conference on Earthquake Engineering, Earthquake Engineering Research Institute.
- Franke, K. W., Rollins, K. M., Ledezma, C., Hedengren, J. D., Wolfe, D., Ruggles, S., Bender, C., and Reimschiissel, B., 2017. Reconnaissance of two liquefaction sites using small unmanned aerial vehicles and structure from motion computer vision following the April 1, 2014 Chile earthquake, *Journal of Geotechnical and Geoenvironmental Engineering*, ASCE **143**, 0406125.
- Galadini, F., Falcucci, E., Gori, S., Zimmaro, P., Cheloni, D., and Stewart, J. P., 2018. Tectonic setting of 2016–2017 Central Italy event sequence and observed source characteristics, *Earthquake Spectra* **34**, 1557–1583. doi:10.1193/101317EQS204M.
- Geotechnical Extreme Events Reconnaissance Association (GEER), 2016a. *Geotechnical aspects of the 2016 Mw 6.2, Mw 6.0, and Mw 7.0 Kumamoto earthquakes* (R. E. Kayen and S. Dashti, eds.), *Geotechnical Extreme Events Reconnaissance Association Report No. GEER-048*. doi:10.18118/G6JS3M.
- Geotechnical Extreme Events Reconnaissance Association (GEER), 2016b. Engineering reconnaissance of the 24 August 2016 central Italy earthquake version 2 (P. Zimmaro and J. P. Stewart, eds.), Geotechnical Extreme Events Reconnaissance Association Report No. GEER-050B. doi:10.18118/G61S3Z.
- Geotechnical Extreme Events Reconnaissance Association (GEER), 2017a. Engineering reconnaissance following the October 2016 central Italy earthquakes version 2 (P. Zimmaro and

- J. P. Stewart, eds.), Geotechnical Extreme Events Reconnaissance Association Report No. GEER-050D. doi:10.18118/G6HS39.
- Geotechnical Extreme Events Reconnaissance Association (GEER), 2017b. Geotechnical reconnaissance of the 2016 Mw 7.8 Kaikoura, New Zealand, earthquake version 1.0 (M. Cubrinovski and J. D. Bray, eds.), Geotechnical Extreme Events Reconnaissance Association Report No. GEER-053. doi:10.18118/G6NK57.
- Hirschmüller, H., 2005. Accurate and efficient stereo processing by semi-global matching and mutual information, *Proceedings, IEEE Conference on Computer Vision and Pattern Recognition* **2**, 807–814.
- Hirschmüller, H., 2008. Stereo processing by semi-global matching and mutual information, *IEEE Transactions on Pattern Analysis and Machine Intelligence* **30**, 328–341.
- Hungr, O., Leroueil, S., and Picarelli, L., 2014. The Varnes classification of landslide types, an update, *Landslides* **11**(2), 167–194.
- Inventario dei Fenomeni Franosi in Italia (IFFI), 2016. Inventario dei Fenomeni Franosi in Italia, available at http://www.progettoiffi.isprambiente.it/cartanetiffi/ (last accessed 2 January 2017; in Italian).
- Instituto Nazionale di Geofisica e Vulcanologia (INGV), 2016. Coseismic displacements for the August 24, 2015 ML6, Amatrice (central Italy) earthquake from the analysis of continuous GPS stations, available at http://ring.gm.ingv.it/?p=1284 (last accessed 17 October 2018).
- Istituto Superiore per la Protezione e la Ricerca Ambientale (ISPRA), 2016. Report attività svolta da ISPRA in data 25-26/08/2016, available at http://www.isprambiente.gov.it/files/notizie-ispra/notizie-2016/sisma-italia-centrale/ReportattivitsvoltadaISPRAindata26.pdf (last accessed 19 October 2016; in Italian).
- Jo, M.-J., Won, J.-S., Kim, S.-W., and Jung, H.-S., 2010. A time-series SAR observation of surface deformation at the southern end of the San Andreas fault zone, *Geosciences Journal* **14**, 277–287.
- Jung, H.-S., Lu, Z., Won, J. S., Poland, M. P., and Miklius, A., 2011. Mapping three-dimensional surface deformation by combining multiple-aperture interferometry and conventional interferometry: Application to the June 2007 eruption of Kilauea volcano, Hawaii, *IEEE Geoscience and Remote Sensing Letters* 8, 34–38.
- Lee, W., Lu, Z., Won, J.-S., Jung, H.-S., and Dzurisin, D., 2013. Dynamic deformation of Seguam Island, Alaska, 1992–2008, from multi-interferogram InSAR processing, *Journal of Volcanology and Geothermal Research* **260**, 43–51.
- Lowe, D. G., 2004. Distinctive image features from scale-invariant keypoints, *International Journal of Computer Vision* **60**, 91–110.
- Lucieer, A., de Jong, S. M., and Turner, D., 2014. Mapping landslide displacements using structure from motion (SfM) and image correlations of multi-temporal UAV photography, *Progress in Physical Geography* **38**, 97–116.
- Marr, D., and Nishihara, H. K., 1978. Representation and recognition of the spatial organization of three-dimensional shapes, in *Proceedings, Royal Society of London B: Biological Sciences* **200**, 269–294.
- Martin, J. G., and Rathje, E. M., 2014. Lateral spread deformations from the 2010–2011 New Zealand earthquake measured from satellite images and optical image correlation, in *Proceedings of the 10th National Conference on Earthquake Engineering*, Earthquake Engineering Research Institute, Oakland, CA.
- Niethammer, U., James, M. R., Rothmund, S., Travelletti, J., and Joswig, M., 2012. UAV-based remote sensing of the Super-Sauze landslide: Evaluation and results, *Engineering Geology* **128**, 2–11.

PAI, 2016. *Carta delle Pericolosità PAI*, available at http://autoritabacini.regione.abruzzo.it/index.php/carta-delle-pericolosita-pai (last accessed 2 January 2017).

- Pix4D SA, 2018. Pix4D, software, available at https://www.pix4d.com/.
- Rathje, E. M., and Adams, B. J., 2008. The role of remote sensing in earthquake science and engineering: Opportunities and challenges, *Earthquake Spectra* **24**(2), 471–492.
- Rathje, E. M., and Carr, L. P., 2010. Satellite observations of landslides caused by the 2008 Wenchuan earthquake in China, in *Proceedings, 9th US National and 10th Canadian Conference on Earthquake Engineering: Reaching Beyond Borders*, 25–29 July 2010, Toronto, Canada.
- Rathje, E. M., and Franke, K. W., 2016. Remote sensing for geotechnical earthquake reconnaissance, *Soil Dynamics and Earthquake Engineering* **91**, 304–316.
- Rathje, E. M., Kayen, R., and Woo, K.-S., 2006. Remote sensing observations of landslides and ground deformation from the 2004 Niigata Ken Chuetsu Earthquake, *Soils Foundation* **46**(6), 831–842.
- Regione Umbria, 2014. Cartografia geologica dell'Umbria: Cartografia geologica vettoriale della Regione Umbria (in Italian), available at http://dati.umbria.it/dataset/carta-geologica-dell-umbria (last accessed 23 January 2018).
- Romeo, S., Di Matteo, L., Melelli, L., Cencetti, C., Dragoni, W., and Fredduzzi, A., 2017. Seismic-induced rockfalls and landslide dam following the October 30, 2016, earthquake in Central Italy, *Landslides* 14, 1457–1465. doi:10.1007/s10346-017-0841-8.
- Ruggles, S., Clark, J., Franke, K. W., Wolfe, D., Hedengren, J. D., Martin, R. A., Reimschiissel, B., and Okeson, T. J., 2016. Comparison of SfM computer vision point clouds of a landslide derived from multiple small UAV platforms and sensors compared to a TLS-based model, *Journal of Unmanned Vehicle Systems*. doi:10.1139/juvs-2015-0043.
- Sextos, A., De Risi, R., Pagliaroli, A., Foti, S., Passeri, F., Ausilio, E., Cairo, R., Capatti, M. C., Chiabrando, F., Chiaradonna, A., Dashti, S., De Silva, F., Dezi, F., Durante, M. G., Giallini, S., Lanzo, G., Sica, S., Simonelli, A. L., and Zimmaro, P., 2018. Local patterns and incremental damage of buildings during the 2016 Central Italy earthquake sequence, *Earthquake Spectra* 34, 1639–1669. doi:10.1193/100317EQS194M.
- Snavely, N., Seitz, S. M., and Szeliski, R., 2008. Modeling the world from internet photo collections, *International Journal of Computer Vision* **80**, 189–210.
- Stumpf, A., Malet, J. P., Kerle, N., Niethammer, U., and Rothmund, S., 2013. Image-based mapping of surface fissures for the investigation of landslide dynamics, *Geomorphology* **186**, 12–27.
- Turner, D., Lucieer, A., and de Jong, S. M., 2015. Time series analysis of landslide dynamics using an unmanned aerial vehicle, *Remote Sensing* 7, 1736–1757.
- Yun, S., Fielding, E. J., Simons, M., Rosen, P., Owen, S., and Webb, F., 2011. *Damage proxy map of February 2011 M6.3 Christchurch earthquake using InSAR coherence*, 8th International Workshop on Advances in the Science and Applications of SAR Interferometry, Frascati, Italy, available at https://earth.esa.int/documents/10174/1567329/Yun_FRINGE2011.pdf (last accessed 8 August 2017).
- Yun, S., Hudnut, K., Owen, S., Webb, F., Simons, M., Sacco, P., Gurrola, E., Manipon, G., Liang, C., Fielding, E. J., Milillo, P., Hua, H., and Coletta, A., 2015. Rapid damage mapping for the 2015 Mw 7.8 Gorkha earthquake using synthetic aperture radar data from COSMO–SkyMed and ALOS-2 Satellites, Seismological Research Letters 86, 1549–1556.
- Zekkos, D., Clark, M., Cowell, K., Medwedeff, W., Manousakis, J., Saraglou, H., and Tsiambaos, G., 2017. Satellite and UAV-enabled mapping of landslides caused by the November 17 2015 Mw 6.5 Lefkada earthquake, in *Proceedings*, 19th International Conference

- on Soil Mechanics and Geotechnical Engineering, International Society of Soil Mechanics and Geotechnical Engineering, London, United Kingdom.
- Zhang, L., Lu, Z., Ding, X., Jung, H.-S., Feng, G., and Lee, C.-W., 2012. Mapping ground surface deformation using temporarily coherent point SAR interferometry: Application to Los Angeles Basin, *Remote Sensing of Environment* 117, 429–439.
- Zimmaro, P., Scasserra, G., Stewart, J. P., Kishida, T., Tropeano, G., Castiglia, M., and Pelekis, P., 2018. Strong ground motion characteristics from 2016 Central Italy earthquake sequence, *Earthquake Spectra* **34**, 1611–1637. doi:10.1193/091817EQS184M.

(Received 21 August 2017; accepted 16 March 2018)